

Dispersity and Architecture Driven Self-assembly and Confined
Crystallization of Symmetric Branched Block Copolymers

Peer-reviewed author version

PITET, Louis; Chamberlain, Bradley; Hauser, Adam & Hillmyer, Marc (2019)
Dispersity and Architecture Driven Self-assembly and Confined Crystallization of
Symmetric Branched Block Copolymers. In: Polymer Chemistry, 10 (39), p. 5385-5395.

DOI: 10.1039/C9PY01173K

Handle: <http://hdl.handle.net/1942/29807>

1 **Dispersity and Architecture Driven Self-assembly and Confined Crystallization of**
2 **Symmetric Branched Block Copolymers**

3 Louis M. Pitet^{†§*}, Bradley M. Chamberlain[‡], Adam W. Hauser[†] and Marc A. Hillmyer^{†*}

4 [†]*Department of Chemistry, University of Minnesota, 207 Pleasant St. SE, Minneapolis,*
5 *Minnesota 55455-0431, United States,* [§]*Institute for Materials Research (IMO) and*

6 *Department of Chemistry, Hasselt University, Martelarenlaan 42, 3500 Hasselt, Belgium*

7 [‡]*Department of Chemistry, Luther College, 700 College Drive, Decorah, Iowa 52101, United*
8 *States*

9 * To whom correspondence should be addressed (e-mail: louis.pitet@uhasselt.be;
10 hillmyer@umn.edu)

11
12 **Abstract**

13 The effect of macromolecular architecture on the morphology and thermal characteristics of
14 triblock copolymers was evaluated for linear, H-shaped, and arachnearm architectures with
15 poly(*cis*-cyclooctene) (PCOE) midblocks flanked with arms of poly(*d,l*-lactide) (PLA). Chain
16 topology was found to significantly influence the interfacial curvature of the microphase
17 separated domains, as implicated by morphological differences observed by transmission
18 electron microscopy (TEM) and small-angle x-ray scattering (SAXS). The branched molecular
19 architectures and molar mass dispersities (\mathcal{D}) of the triblock polymers examined here resulted
20 in a significant shift in the phase boundaries between conventional equilibrium microphase
21 separated structures to higher volume fractions of the end blocks (i.e., PLA) as compared to
22 conventional low dispersity linear triblocks. Macromolecular topology was also found to
23 strongly influence the extent of homo- vs. heterogeneous nucleation in the semi-crystalline
24 PCOE block. The culmination of the bulk phase behavior analysis demonstrates the ability to
25 fine-tune the properties of the block polymers by exploiting different architectures through a
26 synthetically straightforward route.
27

28 INTRODUCTION

29 Macromolecular self-assembly is a powerful tool to tune the design of complex patterns at
30 the nanoscale using bottom-up design principles. Towards this end, block polymers are
31 fascinating hybrid macromolecules comprised of two or more segments of different repeating
32 units connected covalently. Strong enthalpic repulsions between dissimilar blocks drive block
33 polymers to segregate at the nanoscale, and the symmetry and periodicity of the resulting self-
34 assembled morphologies can be precisely tuned through the molar mass (N), composition (f),
35 architecture (linear vs. branched vs. graft), and dispersity, among other factors. Adding more
36 blocks (e.g., as in ABC triblock terpolymers) or altering the connectivity (ABAB... multiblock
37 copolymers) naturally increases the architectural complexity and provides a way to fine-tune
38 the properties and nanoscale patterns typically associated with these systems.¹⁻³ As a result,
39 synthetic pathways toward branched block copolymers have garnered a great deal of attention
40 as an additional route towards complex self-assembled morphologies.⁴⁻¹² Here we explore
41 well-defined symmetric branched block polymers comprising poly(*cis*-cyclooctene) (PCOE)
42 midblocks and poly(*d,l*-lactide) (PLA) end-blocks. The architecture is systematically varied to
43 access linear, H-shaped, and arachnearm architectures. Furthermore, the end and midblocks
44 have disparate molar mass dispersities (\mathcal{D}) owing to the different mechanisms of
45 polymerization (Scheme 1). Detailed synthetic descriptions of such block polymers have been
46 previously reported.¹³

47

48

49

50

51

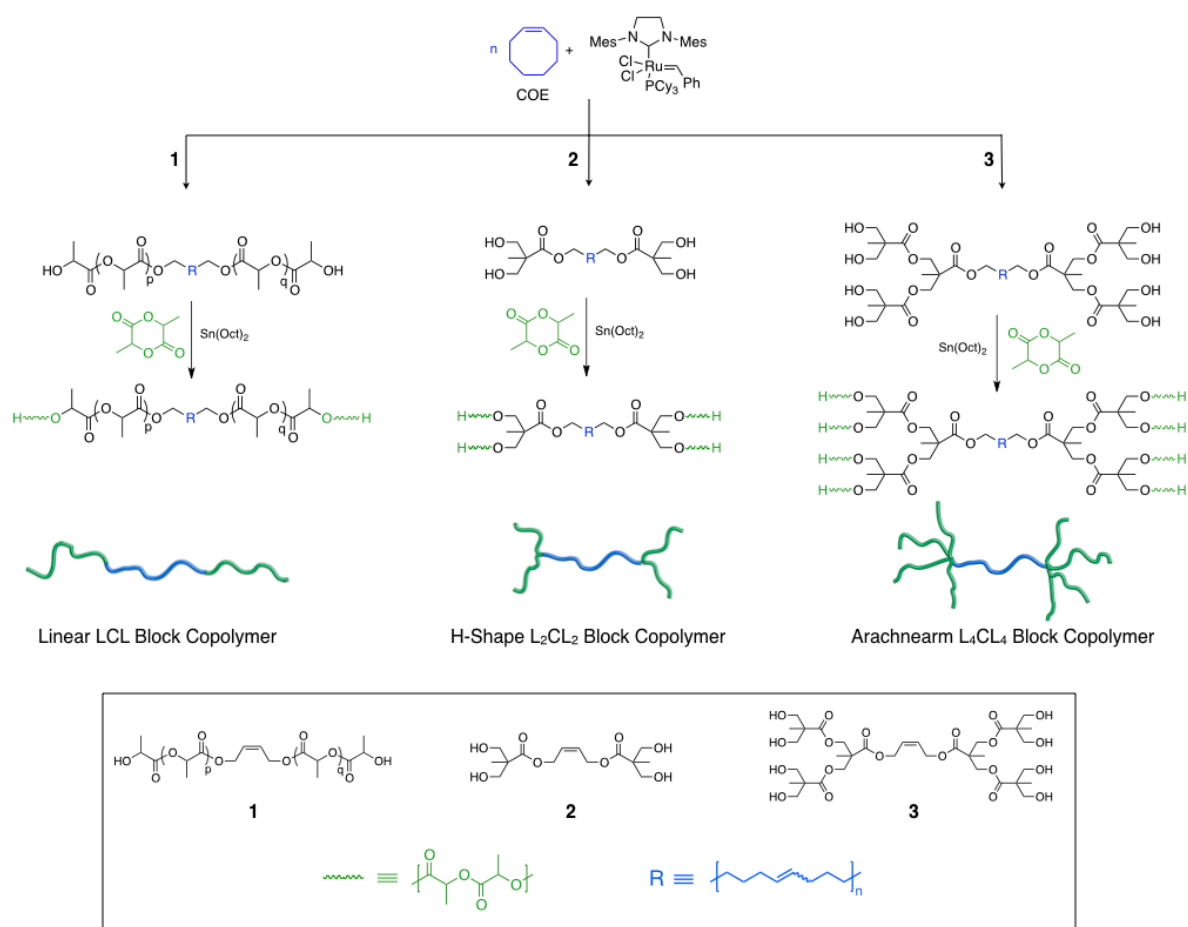
52

53

54

55

56 **Scheme 1.** Synthesis of linear, H-shaped, and arachnearm L_xCL_x symmetric block copolymers



57

58 The influence of branching on the interfacial curvature between the mesoscale phase-
 59 separated domains has been explored theoretically (Figure S1a).¹⁴⁻¹⁷ There are several
 60 reports describing the synthesis of relatively narrow dispersity block copolymers with simple
 61 graft (i.e., A_2B)¹⁸⁻²⁵ and H-shaped (i.e., A_2BA_2)²⁶⁻³⁴ architectures. The general consequence of
 62 branching manifests itself as increased interfacial curvature away from the component with
 63 the greater number of chains converging at the block junctions (i.e., the green PLA component
 64 in Scheme 1). This has significant ramifications on the morphology maps for these systems,
 65 as the composition and arm-asymmetry combined with conformational asymmetry associated
 66 with disparate statistical segment lengths can noticeably shift the microphase boundaries
 67 relative to linear and conformationally symmetric counterparts.³³ The effect of macromolecular
 68 topology on the observed phase behavior can be expressed by the asymmetry parameter (ϵ ,
 69 eq 1).¹⁵

70

71

$$\epsilon = \left(\frac{n_A}{n_B} \right) \left(\frac{\beta_B^2}{\beta_A^2} \right)^{0.5} \quad (1)$$

72

73 where n_i is the number of arms of repeating unit "i" emanating from a block juncture and $\beta_i^2 =$

74 $R_g^2/V = a_i^2/(6v_i)$, [a = statistical segment length; v_i = standard segmental volume; R_g = radius

75 of gyration]. The latter essentially indicates the relative flexibility of a particular component

76 (see Supporting Information, page S9 for a detailed analysis of the statistical parameters

77 associated with PLA and PCOE).³⁵ A conformationally symmetric block copolymer with an A_2B

78 architecture has a value of $\epsilon = 2.0$. As an example of the consequences of architecture on

79 morphology, a linear ABA triblock copolymer with 45 vol % midblock (PCOE here) would be

80 predicted to adopt a lamellar morphology based on self-consistent field theory (SCFT) for $\mathcal{D} =$

81 1.0. However, an analogous branched block polymer with the same composition (45 vol % B-

82 block) but with an A_2B architecture would be expected to adopt cylinders of the B-block, due

83 to an increase in interfacial curvature resulting from contributions of the branched topology to

84 the conformational asymmetry of the graft block polymer.³⁶

85 In addition to the macromolecular topology, molar mass dispersity also affects the phase

86 boundaries in block polymers. The contrasting \mathcal{D} for the two constituent blocks in ABA triblocks

87 (i.e. $\mathcal{D}_A \approx 1$ and $\mathcal{D}_B \approx 2$) typically shifts the morphology map toward higher volume fractions of

88 the midblock compared to the low-dispersity counterparts (Figure S1c).³⁷⁻⁴⁰ For example, the

89 hypothetical linear triblock polymer with 45 vol % midblock that was discussed in the previous

90 paragraph would be expected to adopt a cylindrical morphology rather than a lamellar

91 morphology after accounting for midblock molar mass dispersity. Thus, both of these features

92 (i.e., dispersity and branching) drive the interfacial curvature towards the more disperse PCOE

93 block and away from the branched PLA block, shifting the phase boundaries toward higher

94 volume fraction of midblock (PCOE). The interaction parameter of the PCOE-*b*-PLA system

95 was not reported previously, though the anticipated value is high based on other polyolefin–
96 PLA block copolymers.⁴¹⁻⁴⁷

97 This report evaluates crystallization and bulk phase behavior for symmetric triblock
98 copolymers with varying molecular architectures of the type A_xBA_x , for which $x = 1, 2, \text{ or } 4$.¹³
99 The midblock component was synthesized by ring-opening metathesis polymerization
100 (ROMP) of *cis*-cyclooctene (COE) with a chain-transfer agent to prepare hydroxy-telechelic
101 PCOE. Several different CTAs were used to impart different multiples of hydroxyl functionality
102 to initiate subsequent ring-opening transesterification polymerization (ROTEP) of d,l-lactide
103 and achieve the desired branched block copolymers with linear ($x = 1$), H-shaped ($x = 2$), and
104 arachnearm ($x = 4$) architectures (Scheme 1). The cross-metathesis (i.e., chain-transfer)
105 utilized in the first polymerization gives polymers with molar mass distributions approaching
106 2. Comparatively, ROTEP provides blocks with low dispersity ($D < 1.2$). Both the large molar
107 mass dispersity and the branched architectures can lead to significant deviation from the
108 traditional bulk phase behavior associated with conventional linear block copolymers having
109 near monodisperse size distributions.^{14, 15, 17, 36, 48-56}

110

111 **RESULTS AND DISCUSSION**

112 **Morphological Characterization of Selected Block Copolymers**

113 A series of block copolymers with different architectures was prepared as described
114 previously.¹³ Bulk self-assembly is presented for a select number of samples (Table 1) to
115 exemplify the influence of molecular architecture, whereas crystallization analysis by
116 differential scanning calorimetry (DSC) was performed on all the block copolymers (Table S1).ⁱ
117 Sample identifiers are of the general form $L_xCL_x [\#_x\text{---}\#\text{---}\#_x]$, where x refers to the number of
118 arms emanating from the block junction (i.e., $x = 2 \rightarrow$ H-shaped) and $\#$ refers to the
119 approximate molar mass of the respective segments in kg mol^{-1} .

ⁱ All block copolymers were evaluated with the exception of the H-shaped block copolymer having composition with approximately 15 wt % PLA.

120

121 **Table 1.** Molecular characteristics of several block copolymers prepared for morphological
 122 analysis.

Sample ID	$M_{n,total}^a$	$M_{n,PLA}^b$	w_{PLA}^c	f_{PLA}^d	D_{PCOE}^e	D_{total}^e	morphology ^f	d^{*g}
	kg mol ⁻¹	kg mol ⁻¹						nm
L ₄ CL ₄ [0.4 ₄ -27- 0.4 ₄]	29.9	3.0	0.12	0.09	1.81	1.80	lamellar	26.0
L ₂ CL ₂ [2 ₂ - 23-2 ₂]	29.5	7.0	0.26	0.19	1.71	1.57	lamellar	32.2
LCL [10- 22-10]	41.1	18.6	0.46	0.38	1.70	1.37	lamellar	35.7
L ₂ CL ₂ [5 ₂ - 23-5 ₂]	40.8	18.0	0.46	0.37	1.71	1.38	cylinders (disorganized)	35.5
LCL [21- 22-21]	64.1	41.6	0.66	0.57	1.70	1.27	lamellar	38.5
L ₂ CL ₂ [10 ₂ -23- 10 ₂]	64.5	41.6	0.66	0.57	1.71	1.23	cylinders	30.2

123 ^a Calculated from the M_n (from NMR) of the precursor/macoinitiator PCOE as a reference,
 124 combined with the relative intensities of the respective repeat unit signals obtained from ¹H
 125 NMR spectroscopy. ^b Reported as the total molecular weight of PLA obtained from ¹H NMR
 126 spectroscopy; the molar mass per PLA block can be obtained by dividing by 2 for the linear
 127 copolymers or dividing by 4 for the H-shaped copolymers. ^c Calculated from the relative
 128 intensities of the repeat unit signals in ¹H NMR spectroscopy and using the respective
 129 repeating unit molar mass. ^d Calculated based on the weight fractions and the densities of the
 130 respective components at ambient temperature: $\rho_L = 1.25 \text{ g mL}^{-1}$ (ref. ⁵⁷) and $\rho_C = 0.89 \text{ g mL}^{-1}$
 131 (ref. ⁵⁸). ^e Determined from SEC measurements compared with polystyrene standards. ^f
 132 Determined from the relative position of reflections in SAXS profiles in relation to the principal
 133 scattering vector. ^g Calculated based on the position of the principal scattering vector (q^*) and
 134 the relationship $d^* = 2\pi/q^*$.
 135

136

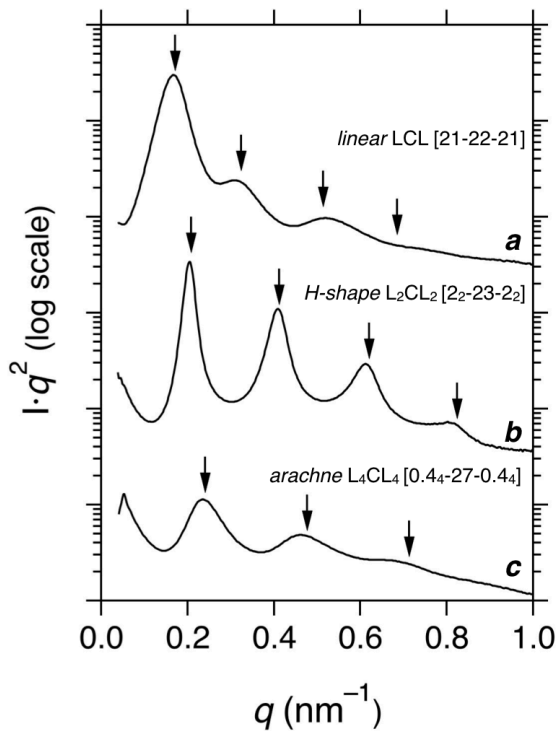
137

138

139 SAXS measurements at 160 °C are shown for three samples having different architectures
 140 and different compositions, yet all exhibiting profiles consistent with lamellar morphologies
 141 (Figure 1). The linear LCL [21-22-21] has a volume fraction of PLA equal to approximately f_L

142 = 0.57 ($f_C = 0.43$) and exhibits a pattern that is characteristic of a lamellar sample with average
 143 domain periodicity ($d^* = 2\pi/q^*$) of 37 nm (Figure 1a). This is well within the calculated lamellar
 144 phase window predicted for a symmetric, linear ABA-type triblock copolymer.

145 In other related work, linear ABA-type triblock copolymers with high- D midblocks were
 146 shown to adopt lamellae between $f_B = 0.25 - 0.48$, representing a substantial shift of the phase
 147 boundaries toward higher volume fraction of disperse midblock.³⁹ This is similar to the system
 148 described here having a rather high- D midblock of PCOE ($D = 1.7$) and relatively low- D PLA
 149 arms. The lamellar morphology is therefore in line with the observations of others and also
 150 with more recent calculations interrogating the effect of block dispersity on phase behavior.⁴⁹
 151



152
 153 **Figure 1.** One-dimensional SAXS profile at 160 °C for (a) the linear block copolymer LCL [21–
 154 22–21] having $f_L = 0.57$; (b) the H-shaped block copolymer L_2CL_2 [2₂-23-2₂] having $f_L = 0.19$
 155 and (c) the arachnearm block copolymer L_4CL_4 [0.4₄-27-0.4₄] having $f_L = 0.09$. Arrows indicate
 156 the predicted positions of Bragg reflections based on the structure factor for a lamellar
 157 morphology related to the position of the primary scattering peak at q^* .

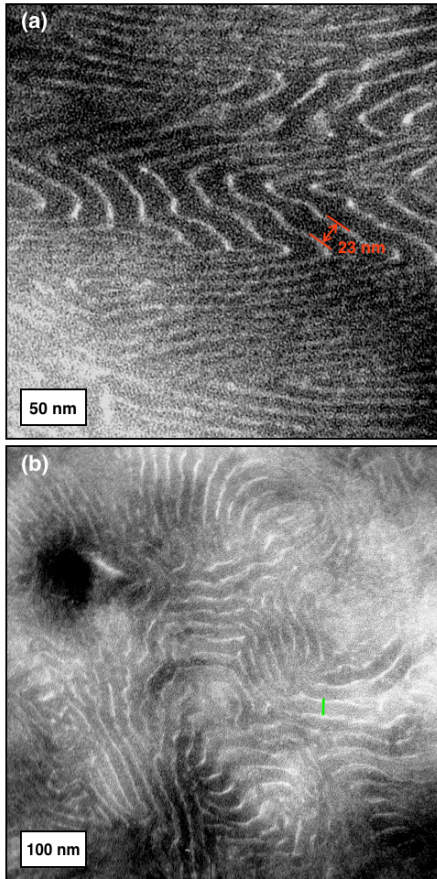
158 The L_2CL_2 [2₂-23-2₂] sample (Table 1) with a volume fraction of PLA (f_L) ≈ 0.19 also
 159 adopted a lamellar morphology as corroborated by TEM (Figure 2) and SAXS analyses
 160 (Figure 1b). The average lamellar spacing is approximately 30 nm as measured by TEM

161 micrographs and is generally consistent with the principal spacing as measured by SAXS (d^*
162 = 32 nm). The average ratio of thickness between the light PLA and dark PCOE layers is
163 approximately 1:4, consistent with the estimated volume fraction of PLA. The observation of
164 a lamellar morphology at such a high volumetric asymmetry was surprising as f_L lies well
165 outside of the typical range where lamellar morphologies are expected in linear ABA triblocks
166 with either low or high D ($D_A = 1.0$; $D_B = 1.5$) (see Figure S1).^{37, 49-51, 59} On the basis of
167 theoretical predictions for the individual parameters (*i.e.*, statistical segment length and
168 dispersities, Eq 1) associated with this system, the branching is likely the largest contributor
169 for the lamellar phase at such high compositional asymmetry.¹⁵ Similarly, lamellar
170 morphologies were observed for linear-dendritic block copolymers having asymmetric
171 compositions that lie outside of the predicted lamellar phase window for linear counterparts.
172 For example linear polystyrene combined with a dendritic poly(benzyl ether) block adopted a
173 lamellar morphology with w_{PS} equal to 0.69⁶⁰ while linear polystyrene combined with dendritic
174 poly(propylene imine) adopted a lamellar morphology when $w_{PS} = 0.75$.⁶¹

175 Finally, the SAXS profile captured at 160 °C for the arachnearm copolymer L₄CL₄ [0.4₄-27-
176 0.4₄] also exhibits a pattern that suggests a lamellar morphology with a domain spacing of d^*
177 = 26 nm. This is the smallest of the periodicities seen for these three samples, despite not
178 having the lowest molar mass. This is further indicative of the impact that branching has on
179 the interfacial geometry. This composition lies far outside the expected phase window for a
180 linear copolymer with high dispersity. While a TEM image was not captured for this sample,
181 morphological assignment is in agreement with the expected morphology for a
182 conformationally symmetric A₄B copolymer based on SCFT (Figure S1).¹⁴

183 The comparison of scattering patterns exhibited by the samples from the three different
184 architectures (linear, H-shaped, arachnearm) suggests that long-range ordering decreases
185 with increasing branching. This is consistent with the observations described for other
186 branched block polymers.⁶² This trend may also have contributed with the increased difficulty
187 of capturing TEM micrographs associated with the arachnearm architectures. Likewise, the

188 SAXS scattering reflections are routinely broader for branched samples than for linear
189 samples throughout this study
190



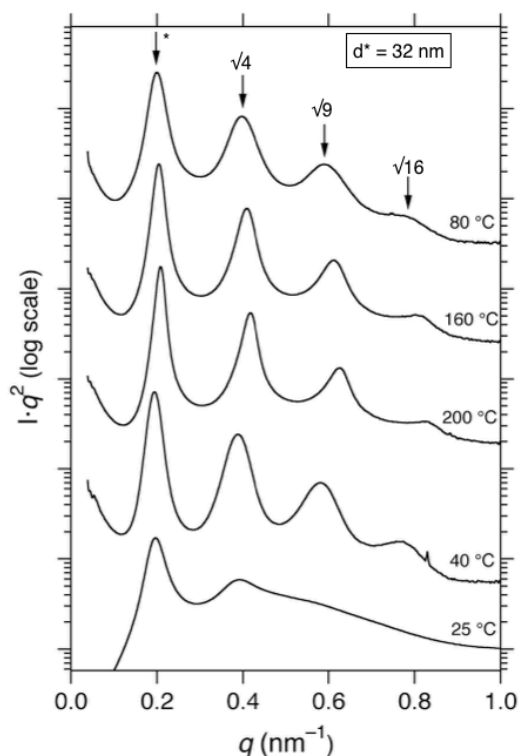
191 **Figure 2.** TEM micrographs for sample L_2CL_2 [2₂-23-2₂] collected at magnifications of (a)
192 $\times 50,000$ and (b) $\times 25,000$. PCOE is stained dark with OsO_4 vapor in the TEM micrographs.
193
194

195 One-dimensional SAXS profiles were collected for L_2CL_2 [2₂-23-2₂] at increasing
196 temperatures during heating in the melt after annealing for approximately 5 minutes at each
197 temperature (Figure 3). Subsequent measurements were then collected upon cooling and
198 annealing at 40 °C and finally at 25 °C. The data are consistent with a lamellar morphology at
199 all temperatures above melting of PCOE ($T_{m,c} = 50$ °C) as indicated by several higher order
200 scattering reflections with strong intensity and maxima occurring at integral multiples of the
201 principal scattering vector q^* . At ambient temperature, the PCOE segment has presumably
202 crystallized, which is responsible for the attenuation of higher order reflections. However, the
203 position and breadth of the principle scattering vector suggests that the morphology has been

204 retained during crystallization (vide infra). The retention of the morphology and the strong
 205 scattering contrast observed in these samples likely arises from the anticipated strong
 206 immiscibility between PLA and hydrocarbon-based polymers, as previously detailed for
 207 systems having similar chemical structures.⁶³

208

209



210

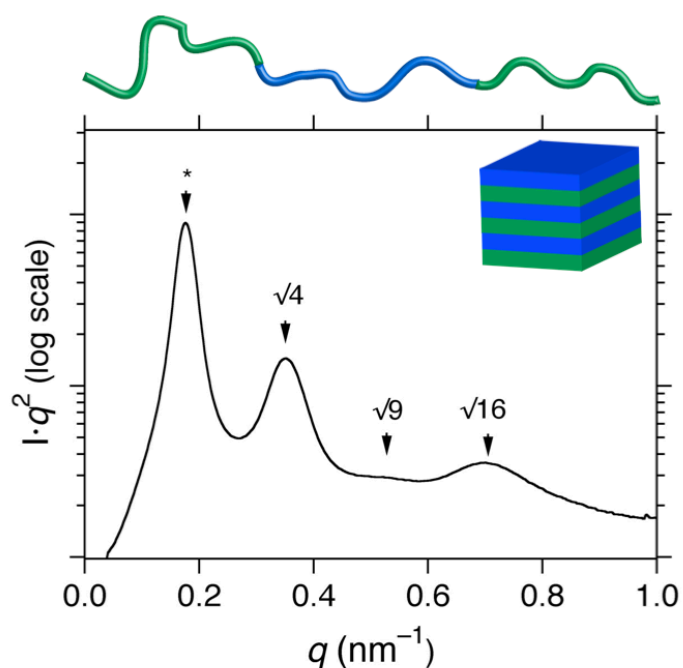
211 **Figure 3.** One-dimensional SAXS profiles For H-shaped block copolymer L_2CL_2 [2₂-23-2₂]
 212 collected at various temperatures in the melt ($T = 80, 160, 200, 40 \text{ }^\circ\text{C} > T_{c,C}$) and crystalline
 213 ($T = 25 \text{ }^\circ\text{C} < T_{m,C}$) states. The top SAXS profile (80 °C) has arrows indicating the position of
 214 the primary scattering peak (q^*) and corresponding predictions for higher order peak positions
 215 associated with Bragg reflections for a lamellar morphology ($\sqrt{4}q^*$, $\sqrt{9}q^*$, $\sqrt{16}q^*$).
 216

217 To more directly examine the effect that macromolecular architecture has on the resulting
 218 self-assembled morphology, a linear LCL triblock (LCL [10-22-10]) was compared to its H-
 219 shaped analog (L_2CL_2 [5₂-23-5₂]) with a nearly identical f_{PLA} yet different chain topology.
 220 Analysis of the linear LCL [10-22-10] ($f_L = 0.38$) by SAXS reveals a profile consistent also
 221 with a lamellar morphology with $d^* = 35.8 \text{ nm}$ (Figure 4). The value of f_L equal to 0.38 falls
 222 within the lamellar window predicted theoretically for an AB diblock copolymer with disparate
 223 D (Figure S1). In contrast, the H-shaped analog of this copolymer, L_2CL_2 [5₂-23-5₂], displayed

224 a morphology consistent with disorganized dispersion of cylindrical-like domains, with $d^* =$
225 35.5 nm based on SAXS and TEM analyses (Figure 5), despite having a nearly identical molar
226 mass and composition as LCL [10-23-10]. Again, this confirms that chain architecture is an
227 important determining factor in the self-assembled morphologies for these triblocks.

228

229



230

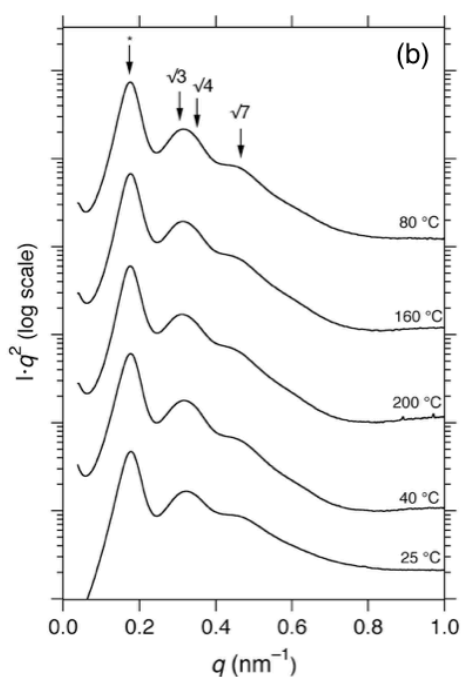
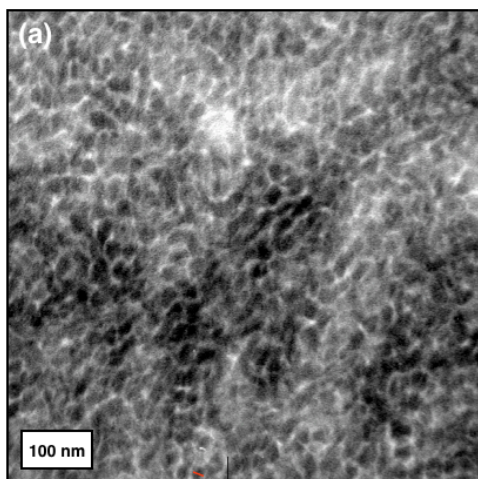
231

232 **Figure 4.** One-dimensional SAXS profile at 25 °C for the linear block copolymer LCL [10–22–
233 10] having $w_L = 0.46$ and $f_L = 0.38$ at ambient temperature as calculated using densities of the
234 respective homopolymers. Arrows indicate the predicted positions of Bragg reflections based
235 on the structure factor for a lamellar morphology related to the position of the primary
236 scattering peak at $q^* = 0.177 \text{ nm}^{-1}$.

237

238

239



240
 241 **Figure 5.** L₂CL₂ [5₂-23-5₂] block copolymer: (a) TEM micrograph showing the darkly stained
 242 (with OsO₄) PCOE domains on the concave side of the domain interfaces and (b) one-
 243 dimensional SAXS profiles at various temperatures with arrows indicating the predicted
 244 positions of Bragg reflections associated with a hexagonally packed cylindrical lattice.
 245

246 A more detailed TEM analysis of the microphase separated domains of L₂CL₂ [5₂-23-5₂]
 247 revealed an array of microdomains with poor long-range spatial correlations, with the stained
 248 PCOE domains situated on the concave side of curved interfaces. This image is not unlike the
 249 morphologies identified by Mahanthappa and coworkers for similarly polydisperse symmetric
 250 triblock copolymers of poly(styrene)-*b*-poly(butadiene)-*b*-poly(styrene).⁶⁴ The authors
 251 described several triblock copolymers with nearly symmetric compositions and observed

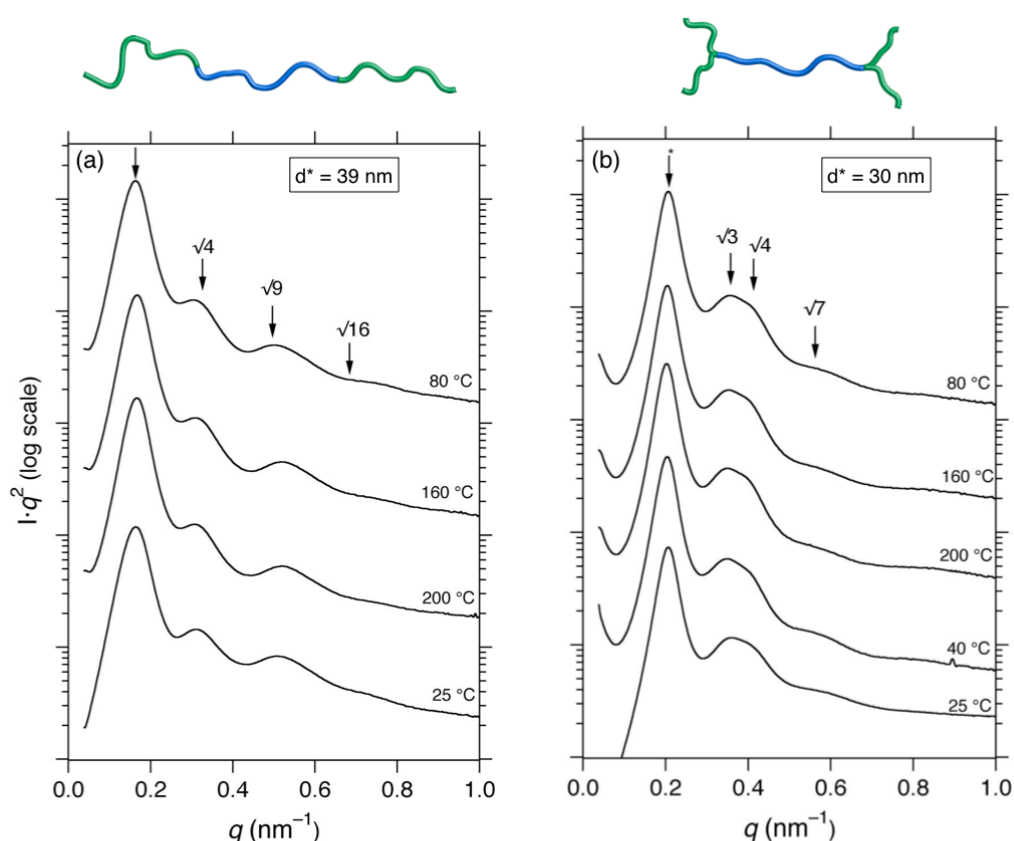
252 molar mass independent adoption of a disordered, bicontinuous morphology. Sample L₂CL₂
253 [5₂-23-5₂] has larger compositional asymmetry than the symmetric counterparts reported by
254 Mahanthappa, with PCOE constituting the majority component by volume. However, based
255 on the TEM micrographs, PLA nevertheless resides predominantly on the convex side of the
256 curved interfaces, suggesting that it occupies the matrix domain. However, a disorganized
257 structure with both components forming continuous paths cannot be ruled out. Linear samples
258 with comparable molar mass and composition to L₂CL₂ [5₂-23-5₂] have been observed to
259 adopt bicontinuous, poorly organized structures in similar systems.³⁸

260 Unambiguous assignment of an ordered morphology is difficult based on SAXS analysis
261 of L₂CL₂ [5₂-23-5₂] (Figure 5b). The patterns suggest distinct microphase separation above
262 the melting temperature (80, 160, 200 °C > $T_{m,c}$) and are consistent with retention of the
263 morphology after cooling below $T_{c,c}$. The primary scattering peak is positioned at $q^* = 0.177$
264 nm⁻¹ at 80 °C ($d = 35.8$ nm). This domain size is nearly identical to the linear analog LCL [10-
265 22-10]. However, the shape and position of higher order reflections for the H-shaped L₂CL₂
266 [5₂-23-5₂] are unique compared with its linear analog. Most notably, a broad reflection
267 centered near $q^*\sqrt{7} = 0.47$ nm⁻¹ is suggestive of a cylindrical morphology. Additionally, the
268 wide breadth of the secondary scattering reflection covers the region in which two other
269 characteristic signals for hexagonally packed cylinders would be anticipated, namely $q^*\sqrt{3}$ and
270 $q^*\sqrt{4}$ (see arrows in Figure 4b). Collectively, these features suggest a hexagonal symmetry,
271 though lacking long-range organization and perhaps mixed with a disordered microphase
272 separated structure as observed by TEM. For the benefit of comparison, we calculated the
273 average cylinder radius (r_c) assuming a well-ordered hexagonal array and the interplanar
274 domain spacing obtained by SAXS with $f_c = 0.63$ at 25 °C, which gave a value $r_c = 12.1$ nm.
275 On the basis of the TEM micrograph in Figure 5a, the average radius of the circular domains
276 ranges from 9-13 nm, which is reasonably consistent with the SAXS analysis.

277 Brief analysis of two additional samples differing only in molecular architecture helps to
278 emphasize the influence that chain topology has on morphology. Namely, linear LCL [21-22-
279 21] and H-shaped L₂CL₂ [10₂-23-10₂] both have $w_L = 0.66$ ($f_L = 0.57$ at 25 °C). SAXS patterns

280 of the linear block copolymer at various temperatures from 25–200 °C are consistent with a
 281 lamellar morphology with d -spacing of 38.5 nm ($q^* = 0.163 \text{ nm}^{-1}$) (Figure 6a). Crystallization
 282 is presumably confined within the lamellar microdomains established in the melt as evinced
 283 by the similitude of profiles taken above and below $T_{c,c}$ (*vide infra*).⁶⁵ This behavior is
 284 consistent with the high T_g of the non-crystallizing PLA block as well as with the expected
 285 large interaction parameter between PLA and PCOE. The lamellar morphology in the linear
 286 triblock falls within a composition range predicted for compositionally symmetric monodisperse
 287 triblock copolymers and polydisperse diblock copolymers. Theoretical treatment of
 288 polydisperse triblock copolymers also illustrates that nearly symmetric composition is
 289 predicted to adopt a morphology with flat interfaces.⁴⁹

290



291

292 **Figure 6.** One dimensional SAXS profiles at various temperatures for (a) linear triblock
 293 copolymer LCL [21–22–21] with $w_L = 0.66$ and $f_L = 0.57$ (at 25 °C) exhibiting higher order
 294 reflections consistent with a lamellar morphology and (b) H-shaped block copolymer L_2CL_2
 295 [10₂–23–10₂] with $w_L = 0.66$ and $f_L = 0.57$ (at 25 °C) exhibiting higher order reflections
 296 consistent with a cylindrical morphology. Morphology assignments are based on the
 297 correlation of reflection positions with the predicted positions of Bragg reflections consistent
 298 with the lattice parameters.

299

300 The H-shaped L₂CL₂ [10₂-23-10₂] exhibits scattering profiles consistent with a hexagonal
301 array of cylinders, despite having a nearly identical composition to the lamellar-forming linear
302 triblock (Figure 6b). There appear clearly demarcated, albeit relatively broad, reflections
303 occurring at multiples of $\sqrt{3}$, $\sqrt{4}$, and $\sqrt{7}$ to the principle scattering peak at $q^* = 0.208 \text{ nm}^{-1}$ at
304 80 °C (above $T_{c,c}$). The small shift in peak position with changing temperature is consistent
305 with the expected dependence of q^* with temperature. Cylinder radius r_c was approximated to
306 be 8.5 nm based on the value $f_c = 0.43$ at 25 °C and the corresponding domain spacing of d^*
307 = 30.2 nm.

308 Comparing the domain spacing obtained from SAXS between the two samples in Figure 6
309 (copolymers L₂CL₂ [10₂-23-10₂] and LCL [21-22-21]) suggests that two different
310 morphologies are adopted. Mean-field approximations predict that a sample exhibiting
311 hexagonally packed cylinders will have a smaller principle domain spacing than a sample with
312 identical molecular weight that adopts a lamellar morphology.⁶⁶ A summary of the
313 morphological features in the selected block copolymers described above is provided in Table
314 1.

315

316 **Crystallization of Branched Block Copolymers**

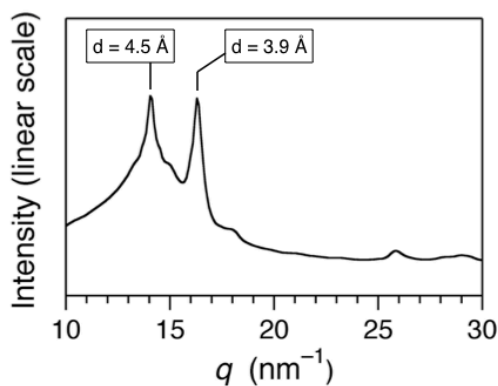
317 Lastly, the bulk morphologies of block copolymers containing at least one semicrystalline
318 component typically exhibit strong path dependence.⁶⁷ The behavior is closely tied to the
319 relative values of T_g of the amorphous component and the T_m of the semicrystalline
320 component. Amorphous PLA exhibits $T_{g,L}$ of approximately 45 °C \pm 5 °C and PCOE is semi-
321 crystalline with $T_{m,C}$ of approximately 55 °C \pm 5 °C and crystallization temperature ($T_{c,C}$) of
322 approximately 35 °C at standard heating/cooling rates of 10 °C min⁻¹.

323 PLA and PCOE block polymers in this study are all expected to occupy the strong
324 segregation regime due to their large estimated interaction parameter, χ .³⁹ Combining strong
325 segregation with the relationship between the relevant transition temperatures ($T_{g,L} > T_{c,C}$)
326 suggests that crystallization occurs within the confined domains of the microphase separated

327 structures established in the melt.^{68, 69} That is, annealing at elevated temperatures ($T \gg T_{m,c}$)
328 followed by cooling at a moderate rate ($\sim 10\text{--}50\text{ }^\circ\text{C min}^{-1}$) should result first in PLA vitrification
329 followed by crystallization of PCOE within the confines templated by the glassy PLA.

330 Indeed, measurement of the SAXS profile of at $25\text{ }^\circ\text{C}$ (bottom profile in Figure 3) shows
331 minimal difference in the intensity and breadth of the primary scattering peak, suggesting that
332 the morphology is preserved upon crystallization. The higher order reflections are less
333 pronounced at ambient temperature than at $T > T_{c,c}$ (where $T_{c,c}$ is the crystallization
334 temperature of PCOE – vide infra) and are dominated by a broad reflection. The broad halo
335 surrounding the intense scattering peak suggests substantial crystallinity, which is consistent
336 with the DSC results ($T_{c,c} \approx 35\text{ }^\circ\text{C}$). The consistent q^* of the scattering reflections suggest that
337 crystallization is confined within the microdomains established in the melt. Crystal confinement
338 is expected on the basis of the relative thermal transitions of the amorphous PLA, which first
339 vitrified and thereby anchored the PCOE chain ends and constrained crystallization within the
340 pre-formed microdomains.^{67, 70} This retention of microphase separation during the
341 crystallization is amplified by the strong segregation strength anticipated for this system.
342 Indeed, wide-angle x-ray scattering (WAXS) profiles collected at $25\text{ }^\circ\text{C}$ show two reflections
343 that are characteristic of a triclinic structure having lattice dimensions of 4.5 and 3.9 Å
344 associated with semi-crystalline PCOE (Figure 7).^{71, 72}

345



346

347 **Figure 7.** One-dimensional WAXS profile for H-shaped block copolymer L₂CL₂ [2₂-23-2₂]
348 collected at ambient temperature.

349

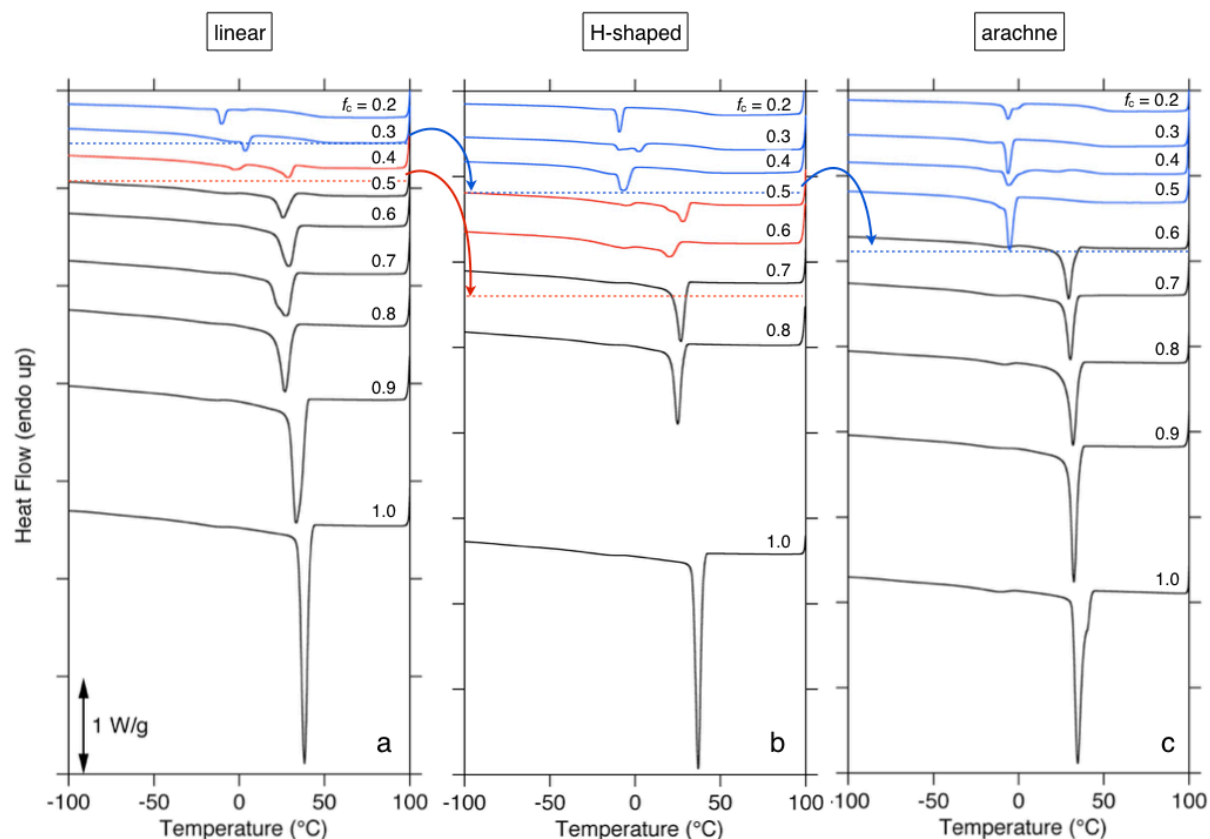
350 Polymer crystallization follows one of two possible mechanisms. In homogeneous
351 nucleation, polymer chains can spontaneously aggregate and align with one another to form
352 a crystallite, thereby serving as a nucleation site from which further crystallization can
353 propagate. In contrast, polymer crystallization may occur from heterogeneous nucleation sites
354 derived from impurities (e.g., catalyst residue, dust). The former case is energetically
355 unfavorable and requires substantial supercooling for crystal nucleation and growth to occur.
356 The latter case is the most energetically favorable, and is the dominant mechanism by which
357 bulk polymers crystallize, since the alternative would require unattainably pristine samples
358 void of impurities.⁷³ However, block copolymers offer a scenario in which homogeneous
359 nucleation may predominate, or alternatively in which multiple crystallization events can take
360 place independently from heterogeneities with different nucleating energy barriers due to
361 confinement of the semi-crystalline block. For example, if the spherical domains described
362 above contain only a few hundred polymeric chains, the probability of an isolated domain
363 experiencing no heterogeneities becomes statistically relevant. Naturally, a considerable
364 portion of the isolated domains may be absent of impurities, and thereby nucleate and
365 crystallize by the homogeneous mechanism. Crystallization exotherms can provide
366 substantive support to this claim; T_c should occur at significantly lower temperature compared
367 with bulk crystallization as a result of the necessary supercooling for homogeneous
368 nucleation.⁷⁴ Multiple crystallization exotherms are sometimes observed as multiple
369 mechanisms may be at play. For example, small domain sizes (e.g., 5–50 nm) may contain
370 several different types of heterogeneities with considerably different energetic barriers to
371 critically nucleate crystallization. However, crystallization in one isolated domain is prevented
372 from propagating through a barrier such as a glassy domain in a microphase separated block
373 copolymer. Likewise, if the semi-crystalline component of a block copolymer occupies a
374 continuous matrix phase, then crystallites nucleated by even a relatively small number of
375 heterogeneities will rapidly propagate throughout the entire material, and a single exotherm is
376 expected in the DSC cooling thermogram. The phenomenon of multiple crystallization
377 mechanisms occurring simultaneously and independently is termed fractionated

378 crystallization,^{75,76} and regularly occurs in block copolymers with semi-crystalline components
379 due to the distinctly small domains accessible as a result of microphase separation.

380 Thermograms from DSC analysis of block copolymers with different architectures and a
381 range of compositions ($f_c = 0.2-1.0$) reveal distinctly different behaviors (Figure 8; Table S1).

382

383



384
385

386 **Figure 8.** DSC cooling thermograms (rate = 10 °C min⁻¹) for block copolymers with a range of
387 compositions with volume fractions of (approximate) PCOE (f_c) from 0.2–1.0 (provided as
388 fractions above the corresponding thermograms) with (a) linear, (b) H-shapedⁱⁱ and (c)
389 arachne arm molecular architectures. Colors correspond to different regimes of crystallization
390 behavior: only heterogeneous nucleation (black), mixed heterogeneous and homogeneous
391 nucleation (red), and only homogeneous nucleation (blue).

ⁱⁱ There is no sample with H-shaped architecture and 90 vol. % PCOE

392

393 The nucleation and crystallization behavior depend on both composition and molecular
394 architecture, which are intimately tied to the morphologies. The minimum in the exotherm occurs
395 nearly identically at $36.5\text{ }^{\circ}\text{C} \pm 2\text{ }^{\circ}\text{C}$ for the three PCOE homopolymers with different end-
396 functionality number (i.e. $\text{HO}_x\text{-PCOE-OH}_x$ with $x = 1, 2, 4$). The thermal behavior of PCOE
397 homopolymers shown in Figure 8a–c are consistent with previous reports (Table S1).^{58, 71} The T_m
398 and T_c both are depressed in the triblock copolymers, in accordance with expectations for strongly
399 segregated systems. The relative position of $T_{c,C}$ (≈ -10 to $+34\text{ }^{\circ}\text{C}$) and $T_{g,L}$ ($\approx +35$ to $+40\text{ }^{\circ}\text{C}$)
400 suggests that crystallization typically occurs after vitrification during cooling, thus anchoring both
401 ends of the PCOE segments during crystallization, and thereby retarding the chain diffusion that
402 occurs during the chain packing associated with crystallization. These topological constraints
403 manifest themselves as depressed T_m and T_c . Nonetheless, a single crystallization exotherm
404 appears for the linear copolymers having f_C from 1.0–0.5 with $T_{c,C}$ ranging from 28–38 $^{\circ}\text{C}$. Two
405 distinct exotherms are observed with minima at 26 $^{\circ}\text{C}$ and $-3\text{ }^{\circ}\text{C}$ for the linear sample with $f_C =$
406 0.4. The sample with f_C equal to 0.3 exhibits a single sharp exotherm centered at $+3\text{ }^{\circ}\text{C}$ with a
407 weak shoulder trailing toward lower temperature. The $T_{c,C}$ being approximately 35 $^{\circ}\text{C}$ lower than
408 the PCOE homopolymer suggests an alternate nucleation mechanism as opposed to a mere
409 artifact of anchored chain ends. Similarly, the sample with f_C equal to 0.2 shows a single exotherm
410 positioned at $-11\text{ }^{\circ}\text{C}$, again suggesting an alternate nucleation mechanism. The $T_{c,C}$ of this
411 particular sample falls nearly 50 $^{\circ}\text{C}$ lower than the $T_{c,C}$ for the bulk PCOE material. The combined
412 thermal results implicate a transition in the bulk morphology adopted in the melt. Specifically, a
413 transition apparently occurs from the sample with $f_C = 0.5$, in which the PCOE occupies a
414 continuous domain, to the sample with $f_C = 0.4$, in which a notable portion of the PCOE occupies
415 isolated domains presumably containing fewer heterogeneities. The isolated domains
416 correspondingly undergo nucleation at greater supercooling. This transition is consistent with the
417 predicted position on the theoretical phase diagram from a lamellar to a cylindrical morphology,

418 with the minority PCOE occupying isolated cylindrical domains. In actuality, the molecular
419 characteristics prohibit the adoption of a well-ordered cylindrical morphology. Instead, the
420 disordered morphological features suggested by the SAXS analysis likely cause a distribution of
421 domain sizes, consistent with the mixed nucleation behavior attributed to the thermogram. Larger
422 asymmetry results in increased curvature of the domain interfaces and therefore larger portions
423 of the PCOE phase occupy isolated domains, accounting for the complete transition to
424 homogeneous nucleation suggested by the thermograms for samples $f_C = 0.3$ and 0.2 .

425 Similar transitions in nucleation behavior are observed for the H-shaped copolymers. However,
426 the boundaries at which the transitions occur are shifted to higher volume fractions of PCOE due
427 to the effects of topological contributions to the conformational asymmetry and thus the interfacial
428 curvature. Complete heterogeneous nucleation and a corresponding single crystallization
429 exotherm centered at $T_{c,C} = 27\text{--}37$ °C are observed for samples with f_C ranging from 1.0 to 0.7,
430 whereas mixed crystallization exotherms occur for samples with f_C equal to 0.6 and 0.5. Single
431 crystallization exotherms with significantly depressed $T_{c,C}$ associated with homogeneous
432 nucleation occur at -6 , -11 and -8 °C in samples with f_C equal to 0.4, 0.3, and 0.2, respectively.
433 Notably, the sample with f_C equal to 0.3 exhibits a multimodal crystallization exotherm with minima
434 occurring at 2 °C and -11 °C, suggesting multiple nucleation mechanisms at work.

435 The boundary representing the transition to complete homogeneous nucleation occurs at a
436 higher value of f_C for the arachnearm block copolymers than for the H-shaped copolymers (Figure
437 8c). There were no arachnearm samples that unambiguously exhibited coexisting nucleation
438 mechanisms. That is, the sample with $f_C = 0.6$ shows a predominant crystallization exotherm
439 occurring at $T_{c,C} = 30$ °C, whereas the sample with $f_C = 0.5$ has a predominant exotherm with $T_{c,C}$
440 $= -6$ °C, a difference of 36 °C. Comparatively, the transition to predominantly homogeneous
441 nucleation occurs between values of $f_C = 0.5$ and 0.6 for the arachnearm architecture, between f_C
442 $= 0.4$ and 0.5 for the H-shaped architecture, and between $f_C = 0.3$ and 0.4 for the linear block
443 copolymers. These results are consistent with the phase boundary shifts predicted by Milner for

444 asymmetrically branched block copolymers.¹⁵ The system accommodates the increasing
445 energetic requirements for relaxing the PLA chains as the junction functionality increases by
446 adjusting the curvature of the domain interfaces such that PLA occupies the convex side. The
447 highly asymmetric arachnearm architecture, for example, presumably transitions to a spherical-
448 like morphology at higher volume fractions than the less branched counterparts, which manifests
449 itself as a transition to a homogeneous nucleation mechanism. This behavior is consistent with
450 the DSC data associated with large supercoolings that result from the large proportion of small,
451 isolated domains containing the semi-crystalline PCOE.

452

453 **CONCLUSION**

454 The bulk phase behavior has been described for several block copolymers with ABA linear
455 architecture and A₂BA₂ H-shaped and A₄BA₄ arachnearm architectures at various compositions.
456 Direct imaging of several samples revealed different morphologies adopted by the block
457 copolymers as a function of branch functionality, with the curvature of the domain interfaces
458 showing a strong dependence on both composition and molecular architecture. Specifically, a
459 lamellar morphology was observed at highly asymmetric compositions ($f_L = 0.19$) for an H-shaped
460 block copolymer. Likewise, two corresponding copolymers with linear and H-shaped architectures
461 exhibited SAXS profiles characteristic of lamellar and cylindrical morphologies, respectively, with
462 $f_L = 0.57$. Lastly, the crystallization behavior for a broad range of compositions was evaluated for
463 linear, H-shaped, and arachnearm architectures, showing a strong dependence of nucleation
464 mechanism on extent of branching. The crystallization behavior corroborates the observed phase
465 behavior monitored by SAXS and TEM.

466 Collectively, we have demonstrated that architectural complexity can be utilized in PLA block
467 copolymers to access morphologies that are inaccessible with conventional linear block
468 copolymers. Importantly, the complexity was bestowed by using straightforward polymerization
469 techniques; identical conditions were used to prepare the different architectures using

470 conventional techniques with commercially available starting materials. Using this protocol, the
471 mechanical and thermal properties of PLA block copolymers can be fine-tuned to the specific
472 demands of various applications.

473

474 **CONFLICTS OF INTEREST**

475 There are no conflicts to declare.

476

477 **ACKNOWLEDGMENTS**

478 This work was funded by the National Science Foundation (DMR-0605880 and DMR-1006370
479 and DMR-1609459). L.M.P. acknowledges support from a fellowship awarded by the UMN
480 Graduate School. B.M.C gratefully acknowledges the Office of the Dean at Luther College for
481 financial support of a sabbatical leave of absence. Parts of this work were carried out at the
482 University of Minnesota Characterization Facility, a member of the NSF-funded Materials
483 Research Facilities Network (www.mrfn.org). Synchrotron SAXS analyses were conducted at the
484 DuPont–Northwestern–Dow Collaborative Access Team (DND-CAT) located at Sector 5 of the
485 Advanced Photon Source (APS), supported by E.I. DuPont de Nemours & Co., the Dow Chemical
486 Company, and Northwestern University. Use of the APS, an Office of Science User Facility
487 operated for the U.S. Department of Energy (DOE) Office of Science by Argonne National
488 Laboratory, was supported by the U.S. DOE under Contract DE-AC02-06CH11357. We are
489 grateful for careful reviewing of the manuscript by Nicholas Hampu and Claire Dingwell.

490

491 Electronic Supplementary Information (ESI) available: [details of any supplementary
492 information available should be included here]. See DOI: 10.1039/x0xx00000x

493

494 **REFERENCES**

- 495 1. F. S. Bates, M. A. Hillmyer, T. P. Lodge, C. M. Bates, K. T. Delaney and G. H. Fredrickson,
496 *Science*, 2012, **336**, 434-440.
- 497 2. N. Hadjichristidis, M. Pitsikalis and H. Iatrou, *Adv. Polym. Sci.*, 2005, **189**, 1-124.
- 498 3. H. Feng, X. Lu, W. Wang, N.-G. Kang and J. W. Mays, *Polymers*, 2017, **9**, 494.
- 499 4. Y. Deng, S. Zhang, G. Lu and X. Huang, *Polym. Chem.*, 2013, **4**, 1289-1299.
- 500 5. B. A. Temel, J. Amici, M. Sangermano and Y. Yagci, *J. Polym. Sci., Part A: Polym. Chem.*,
501 2013, **51**, 4601-4607.
- 502 6. X. Fan, Z. Wang, D. Yuan, Y. Sun, Z. Li and C. He, *Polym. Chem.*, 2014, **5**, 4069-4075.
- 503 7. B. V. K. J. Schmidt, M. Hetzer, H. Ritter and C. Barner-Kowollik, *Prog. Polym. Sci.*, 2014, **39**,
504 235-249.
- 505 8. F. Wurm and H. Frey, *Prog. Polym. Sci.*, 2011, **36**, 1-52.
- 506 9. M. Pitsikalis, S. Pispas, J. W. Mays and N. Hadjichristidis, *Adv. Polym. Sci.*, 1998, **135**, 1-
507 137.
- 508 10. N. Hadjichristidis, M. Pitsikalis, S. Pispas and H. Iatrou, *Chem. Rev.*, 2001, **101**, 3747-3792.
- 509 11. N. Hadjichristidis, H. Iatrou, M. Pitsikalis and J. Mays, *Prog. Polym. Sci.*, 2006, **31**, 1068-
510 1132.
- 511 12. A. Hirao, K. Murano, T. Oie, M. Uematsu, R. Goseki and Y. Matsuo, *Polym. Chem.*, 2011, **2**,
512 1219-1233.
- 513 13. L. M. Pitet, B. M. Chamberlain, A. W. Hauser and M. A. Hillmyer, *Macromolecules*, 2010, **43**,
514 8018-8025.
- 515 14. M. W. Matsen, *Macromolecules*, 2012, **45**, 2161-2165.
- 516 15. S. T. Milner, *Macromolecules*, 1994, **27**, 2333-2335.
- 517 16. C.-I. Huang and L.-F. Yang, *Macromolecules*, 2010, **43**, 9117-9125.
- 518 17. N. A. Lynd, F. T. Oyerokun, D. L. O'ÄDonoghue, D. L. Handlin and G. H. Fredrickson,
519 *Macromolecules*, 2010, **43**, 3479-3486.
- 520 18. G. Floudas, N. Hadjichristidis, H. Iatrou, T. Pakula and E. W. Fischer, *Macromolecules*, 1994,
521 **27**, 7735-7746.
- 522 19. G. Floudas, N. Hadjichristidis, H. Iatrou and T. Pakula, *Macromolecules*, 1996, **29**, 3139-
523 3146.
- 524 20. N. Hadjichristidis, H. Iatrou, S. K. Behal, J. J. Chludzinski, M. M. Disko, R. T. Garner, K. S.
525 Liang, D. J. Lohse and S. T. Milner, *Macromolecules*, 1993, **26**, 5812-5815.

- 526 21. D. J. Pochan, S. P. Gido, S. Pispas and J. W. Mays, *Macromolecules*, 1996, **29**, 5099-5105.
- 527 22. D. J. Pochan, S. P. Gido, S. Pispas, J. W. Mays, A. J. Ryan, J. P. A. Fairclough, I. W. Hamley
528 and N. J. Terrill, *Macromolecules*, 1996, **29**, 5091-5098.
- 529 23. M. R. Whittaker, C. N. Urbani and M. J. Monteiro, *J. Am. Chem. Soc.*, 2006, **128**, 11360-
530 11361.
- 531 24. C. Dyer, P. Driva, S. W. Sides, B. G. Sumpter, J. W. Mays, J. Chen, R. Kumar, M. Goswami
532 and M. D. Dadmun, *Macromolecules*, 2013, **46**, 2023-2031.
- 533 25. T. Isono, I. Otsuka, Y. Kondo, S. Halila, S. Fort, C. Rochas, T. Satoh, R. Borsali and T.
534 Kakuchi, *Macromolecules*, 2013, **46**, 1461-1469.
- 535 26. G. Floudas, N. Hadjichristidis, H. Iatrou, A. Avgeropoulos and T. Pakula, *Macromolecules*,
536 1998, **31**, 6943-6950.
- 537 27. Y.-G. Li, P.-J. Shi and C.-Y. Pan, *Macromolecules*, 2004, **37**, 5190-5195.
- 538 28. Y. Cong, B. Li, Y. Han, Y. Li and C. Pan, *Macromolecules*, 2005, **38**, 9836-9846.
- 539 29. J. Liu and C.-Y. Pan, *Polymer*, 2005, **46**, 11133-11141.
- 540 30. D.-H. Han and C.-Y. Pan, *J. Polym. Sci., Part A: Polym. Chem.*, 2006, **44**, 2794-2801.
- 541 31. A. Ekin and D. C. Webster, *Macromolecules*, 2006, **39**, 8659-8668.
- 542 32. T. Higashihara, R. Faust, K. Inoue and A. Hirao, *Macromolecules*, 2008, **41**, 5616-5625.
- 543 33. Y. H. Wei, B. Y. Li, Y. C. Han and C. Y. Pan, *Soft Matter*, 2008, **4**, 2507-2512.
- 544 34. C. Detrembleur, A. Debuigne, O. Altintas, M. Conradi, E. H. H. Wong, C. Jerome, C. Barner-
545 Kowollik and T. Junkers, *Polym. Chem.*, 2012, **3**, 135-147.
- 546 35. P. A. Weimann, T. D. Jones, M. A. Hillmyer, F. S. Bates, J. D. Londono, Y. Melnichenko, G.
547 D. Wignall and K. Almdal, *Macromolecules*, 1997, **30**, 3650-3657.
- 548 36. C. Lee, S. P. Gido, Y. Poulos, N. Hadjichristidis, N. B. Tan, S. F. Trevino and J. W. Mays, *J.*
549 *Chem. Phys.*, 1997, **107**, 6460-6469.
- 550 37. M. W. Matsen and R. B. Thompson, *J. Chem. Phys.*, 1999, **111**, 7139-7146.
- 551 38. J. M. Widin, A. K. Schmitt, A. L. Schmitt, K. Im and M. K. Mahanthappa, *J. Am. Chem. Soc.*,
552 2012, **134**, 3834-3844.
- 553 39. A. K. Schmitt and M. K. Mahanthappa, *Macromolecules*, 2014, **47**, 4346-4356.
- 554 40. A. K. Schmitt and M. K. Mahanthappa, *Macromolecules*, 2017, **50**, 6779-6787.
- 555 41. Y. Wang and M. A. Hillmyer, *J. Polym. Sci., Part A: Polym. Chem.*, 2001, **39**, 2755-2766.
- 556 42. Y. Wang and M. A. Hillmyer, *Macromolecules*, 2000, **33**, 7395-7403.

- 557 43. N. A. Lynd and M. A. Hillmyer, *Macromolecules*, 2007, **40**, 8050–8055.
- 558 44. N. A. Lynd and M. A. Hillmyer, *Macromolecules*, 2005, **38**, 8803-8810.
- 559 45. K. S. Anderson, K. M. Schreck and M. A. Hillmyer, *Polym. Rev.*, 2008, **48**, 85-108.
- 560 46. K. S. Anderson, S. H. Lim and M. A. Hillmyer, *J. Appl. Polym. Sci.*, 2003, **89**, 3757-3768.
- 561 47. K. S. Anderson and M. A. Hillmyer, *Polymer*, 2004, **45**, 8809-8823.
- 562 48. E. W. Cochran, C. J. Garcia-Cervera and G. H. Fredrickson, *Macromolecules*, 2006, **39**,
563 2449-2451.
- 564 49. M. W. Matsen, *Eur. Phys. J. E: Soft Matter*, 2013, **36**, 1-7.
- 565 50. M. W. Matsen, *Eur. Phys. J. E: Soft Matter*, 2006, **21**, 199-207.
- 566 51. M. W. Matsen, *Phys. Rev. Lett.*, 2007, **99**, 148304/148301-148304/148304.
- 567 52. N. A. Lynd, A. J. Meuler and M. A. Hillmyer, *Prog. Polym. Sci.*, 2008, **33**, 875-893.
- 568 53. S. T. Milner, T. A. Witten and M. E. Cates, *Macromolecules*, 1989, **22**, 853-861.
- 569 54. M. Nadgorny, D. T. Gentekos, Z. Y. Xiao, S. P. Singleton, B. P. Fors and L. A. Connal,
570 *Macromol. Rapid Commun.*, 2017, **38**, 1700352.
- 571 55. D. T. Gentekos and B. P. Fors, *Acs Macro Letters*, 2018, **7**, 677-682.
- 572 56. D. T. Gentekos, J. T. Jia, E. S. Tirado, K. P. Barteau, D. M. Smilgies, R. A. DiStasio and B.
573 P. Fors, *J. Am. Chem. Soc.*, 2018, **140**, 4639-4648.
- 574 57. D. R. Witzke, J. J. Kolstad and R. Narayan, *Macromolecules*, 1997, **30**, 7075-7085.
- 575 58. W. A. Schneider and M. F. Müller, *J. Mol. Catal.*, 1988, **46**, 395–403.
- 576 59. J. M. Widin, M. Kim, A. K. Schmitt, E. Han, P. Gopalan and M. K. Mahanthappa,
577 *Macromolecules*, 2013, **46**, 4472-4480.
- 578 60. M. E. Mackay, Y. Hong, M. Jeong, B. M. Tande, N. J. Wagner, S. Hong, S. P. Gido, R.
579 Vestberg and C. J. Hawker, *Macromolecules*, 2002, **35**, 8391-8399.
- 580 61. C. Román, H. R. Fischer and E. W. Meijer, *Macromolecules*, 1999, **32**, 5525-5531.
- 581 62. H. Wang, W. Lu, W. Wang, P. N. Shah, K. Misichronis, N.-G. Kang and J. W. Mays,
582 *Macromol. Chem. Phys.*, 2018, **219**, 1700254.
- 583 63. S. C. Schmidt and M. A. Hillmyer, *J. Polym. Sci., Part B: Polym. Phys.*, 2002, **40**, 2364-2376.
- 584 64. J. M. Widin, A. K. Schmitt, K. Im, A. L. Schmitt and M. K. Mahanthappa, *Macromolecules*,
585 2010, **43**, 7913-7915.
- 586 65. Y.-L. Loo, R. A. Register and A. J. Ryan, *Macromolecules*, 2002, **35**, 2365-2374.

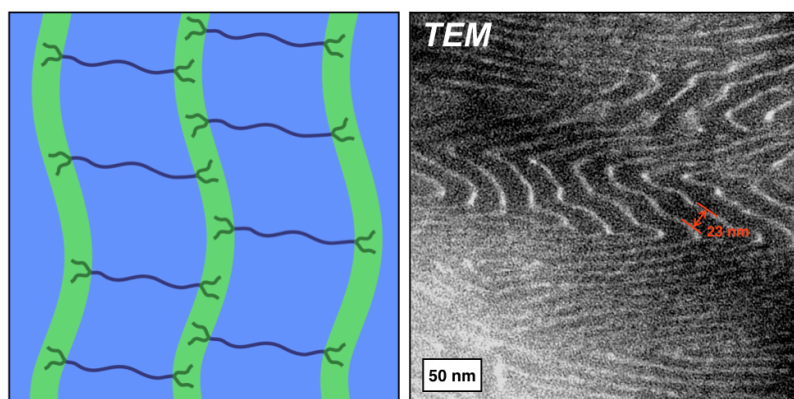
- 587 66. M. W. Matsen and F. S. Bates, *J. Chem. Phys.*, 1997, **106**, 2436-2448.
- 588 67. Y.-L. Loo, R. A. Register, A. J. Ryan and G. T. Dee, *Macromolecules*, 2001, **34**, 8968-8977.
- 589 68. I. W. Hamley, *Adv. Polym. Sci.*, 1999, **148**, 114-137.
- 590 69. A. J. Muller, V. Balsamo and M. L. Arnal, *Adv. Polym. Sci.*, 2005, **190**, 1-63.
- 591 70. D. J. Quiram, R. A. Register and G. R. Marchand, *Macromolecules*, 1997, **30**, 4551-4558.
- 592 71. C. Liu, S. B. Chun, P. T. Mather, L. Zheng, E. H. Haley and E. B. Coughlin, *Macromolecules*,
593 2002, **35**, 9868-9874.
- 594 72. I. W. Bassi and G. Fagherazzi, *Eur. Polym. J.*, 1968, **4**, 123-132.
- 595 73. P. J. Barham, D. A. Jarvis and A. Keller, *J. Polym. Sci., Part B: Polym. Phys.*, 1982, **20**, 1733-
596 1748.
- 597 74. O. O. Santana and A. J. Mueller, *Polym. Bull.*, 1994, **32**, 471-477.
- 598 75. H. Frensch, P. Harnischfeger and B. J. Jungnickel, *Acs Symposium Series*, 1989, **395**, 101-
599 125.
- 600 76. H. Frensch and B. J. Jungnickel, *Colloid and Polymer Science*, 1989, **267**, 16-27.
601
602

603 TOC Graphic for:

604 **Dispersity and Architecture Driven Bulk Phase Behavior and Confined Crystallization In**
605 **Symmetric Branched Block Copolymers Containing Polylactide and Polycyclooctene**

606 Louis M. Pitet, Bradley M. Chamberlain, Adam W. Hauser and Marc A. Hillmyer

607



608 *Highly asymmetric lamellae from disperse branched block copolymers*

609